NASA TN D-1023

TECHNICAL NOTE

D-1023

TRANSONIC FLUTTER TESTS OF A HIGHLY SWEPT ARROW WING WITH AND WITHOUT SIMULATED TRAILING-EDGE-MOUNTED ENGINE MASSES

By Gerald D. Walberg

Langley Research Center
Langley Air Force Base, Va.

NATIONAL AERONAUTICS AND SPACE ADMINISTRATION

WASHINGTON March 1962

NATIONAL AERONAUTICS AND SPACE ADMINISTRATION

TECHNICAL NOTE D-1023

TRANSONIC FLUTTER TESTS OF A HIGHLY SWEPT ARROW WING WITH AND WITHOUT SIMULATED TRAILING-EDGE-MOUNTED ENGINE MASSES

By Gerald D. Walberg

SUMMARY

Transonic flutter tests were made for three series of cantilevered semispan wing models which had arrow planforms and leading-edge sweep angles of 72.5°. The first series were basic wing panels; the second series carried simulated engine masses and nacelles located at 34.9, 55.8, and 76.6 percent of the semispan; the third series carried only lightweight nacelles. The mass of each simulated engine was approximately 41 percent of the basic wing-panel mass. At Mach numbers below 0.975, the addition of the engine masses increased the flutter dynamic pressure of the basic wings; the nacelles do not affect the flutter boundary of the basic wings in this Mach number range. At Mach numbers above 1.05 the flutter boundary for the wings with engine masses and nacelles was higher than the boundary of the basic wings, but below the boundary for the wings with only lightweight nacelles.

INTRODUCTION

Among the designs presently being considered for a supersonic transport is a configuration which features a highly swept arrow wing carrying engines mounted along the trailing edge. The placement of large masses along a wing trailing edge raises questions regarding the flutter characteristics of the wing. Previous investigations have shown that, for wings of moderate sweep angle, a mass mounted along the trailing edge usually produces a reduction in the dynamic pressure required for flutter at subsonic and transonic Mach numbers. (See, for example, refs. 1 to 4.) Presently, few data are available regarding the effects of localized trailing-edge-mounted masses on the flutter characteristics of arrow wings having large sweep angles.

Accordingly, an exploratory investigation has been carried out in the Langley 8-foot transonic pressure tunnel to determine the transonic flutter characteristics of a cantilevered semispan arrow wing which had

a leading-edge sweep angle of 72.5°. Three series of models were tested. The models of series I were basic wings with no nacelles; those of series II carried simulated engine masses and nacelles; series III models carried only lightweight nacelles. The results of this investigation are reported herein.

SYMBOLS

A	wing aspect ratio
b_0	streamwise root semichord, ft
$c(\eta)$	local streamwise chord, in.
$c'(\eta)$	local chord parallel to wing-root flange, in.
f	frequency of vibration, cps
g	structural damping coefficient as determined by logarithmic decrement method
l	semispan, ft
l'	perpendicular distance from wing-root flange to wing tip, in.
M	Mach number
$m\left(\frac{x}{c},\eta\right)$	local mass per unit area, slugs/sq ft
q	dynamic pressure, lb/sq ft
r	local fuselage radius, in. (fig. 2)
S	full-span planform area, sq ft
t	wing-skin thickness, in.
V	velocity of airstream, ft/sec
v	volume of a truncated cone of height l' and diameter $c'(\eta)$
x	distance from wing leading edge, nacelle nose, or fuselage nose, positive rearward, in. (fig. 2)

$y\left(\frac{x}{c}\right)$ local half thickness of streamwise airfoil section, in. (fig. 2)

η nondimensional semispan length, $\frac{\text{Distance along semispan}}{l}$

μ panel mass ratio, ratio of wing-panel mass (including engine and nacelle masses) to mass of a truncated cone of air having height l', diameter $c'(\eta)$, and density ρ

ρ density of airstream, slugs/cu in.

ρ_c density of wing core, slugs/cu in.

ρ_s density of wing-skin—glue-joint combination, slugs/cu in.

ω circular frequency of vibration, $2\pi f$, radians/sec

Subscripts:

f conditions at flutter

i pertaining to ith natural vibration mode, i = 1,2,3,4

MODELS

The models used in the present investigation were generalized research models and were not dynamically scaled to represent a particular transport configuration. The models did, however, have planform, engine placement, and nacelle designs similar to one version of the configuration mentioned in reference 5 (p. 53, fig. 8).

Model Designation

Three series of models were tested. All these models had the same basic structure, planform, and airfoil section. The models of series I were basic wings; those of series II carried simulated engine masses and nacelles; the models of series III carried only lightweight nacelles. Each model designation is comprised of a Roman and an Arabic numeral. The Roman numeral refers to the series of the model, and the Arabic numeral refers to the number of the model within the series.

Model Geometry and Construction

Figure 1 presents structural and geometric details of the models used in this investigation. The basic model had a full-span aspect ratio of 2.29 and a leading-edge sweepback angle of 72.5°. The ordinates of the airfoil section, which was constant along the span, are given in figure 2. The models of series II and III carried simulated engine nacelles. These nacelles were bodies of revolution, designed to have the same area distribution as the nacelles of the configuration in reference 1. Nacelle ordinates are presented in figure 2. The series II models carried simulated engine masses located at 34.9, 55.8, and 76.6 percent of the semispan. The mass center of each simulated engine was located at the trailing edge of the wing.

Natural vibration modes and frequencies.- The first four natural frequencies of vibration and their associated node lines and structural damping coefficients were determined for each model. The models were excited with a small air shaker. Once a natural mode had been located, the node line was located by sprinkling carborundum grit on the wing surface. Decay records were used to determine structural damping coefficients. Natural frequencies and structural damping coefficients are presented in table II. Nodal patterns are presented in figure 3.

From the node lines presented in figure 3, it may be seen that the natural mode shapes of all the models in series I and III are nearly identical. Accordingly, natural mode shapes were measured from model I1 and are considered representative of all the wings in series I and III. Similarly, natural mode shapes were measured from model II5 and are considered representative of the series II models. The first four natural modes for these representative wings (I1 and II5) are presented in figure 4. The method used in determining the natural mode shapes is described in reference 6. In applying this method, 1/16-inch-square mirrors were glued to the wing surface at 0, 25, 50, 75, and 100 percent of the local streamwise chord and at 20, 40, 60, 80, and 100 percent of the semispan. Light from a point source was reflected by the mirrors onto a screen. The light source and screen were located 151 inches from the mean surface of the wing. During vibration in a natural mode, the images reflected from the mirrors appeared as straight lines whose lengths and directions were marked on the screen. These lines were resolved into components indicative of the local pitching and rolling slopes of the mean surface of the wing. These slopes were then integrated numerically to yield the desired natural mode shapes.

The primary load-carrying structure of the models was the wing skin. This skin was a fiber-glass-plastic laminate, made from two layers of 0.003-inch-thick glass cloth. The wing skins were bonded to a foam plastic core, which served to stabilize them against buckling. An aluminum mounting block was bonded to the wing root. Cylindrical lead slugs

were used to simulate the engine masses. The engine nacelles were hollowed from balsa wood and had wall thicknesses of approximately 1/32 inch.

Physical Properties of Models

Mass properties.- Mass properties of the models are presented in table I. The complete panel mass of each model is the mass of the portion of the wing outboard of the wing-root flange. Panel masses, engine masses, and nacelle masses were determined by weighing each item individually. The densities of the plastic cores were determined by weighing each core prior to assembling the model and then dividing these measured masses by the calculated core volume. Skin mass was computed by subtracting the core, engine, and nacelle masses from the panel mass and then dividing the resultant skin mass by the calculated skin volume. The skin mass includes both the mass of the skin itself and of the glue joint between the skin and the core. Due to the simple construction of the models, the mass distribution of the basic panel (excluding engine and nacelle masses) may be computed as

$$m = \rho_c c\left(\frac{2y}{c}\right) + 2\rho_s t$$

where

$$m = m\left(\frac{x}{c}, \eta\right)$$

$$c = c(\eta)$$

$$\frac{y}{c} = \frac{y}{c}\left(\frac{x}{c}\right)$$

and where m is the panel mass per unit area, ρ_c and ρ_s are the core and skin densities, respectively, c is the local streamwise chord, y/c is the local airfoil ordinate (in percent streamwise chord), and t is the skin thickness. The airfoil ordinates y/c are presented in figure 2, and t was found to be 0.008 inch for the models.

Instrumentation

The models were instrumented with electrical strain gages. Two-active-arm bridges of bending and torsion gages were located near the

50-percent-chord line at 30 percent of the semispan. During the tests a tape recorder was used to record the signals from the gages. These records were used to determine flutter frequencies and the onset of flutter. The strain-gage signals were also fed into a cathode-ray oscilloscope in such a way that a Lissajous pattern indicated the start of flutter. At each test point the tunnel Mach number, stagnation temperature, and stagnation pressure were recorded by a punchcard readout system.

TUNNEL AND MODEL MOUNTING SYSTEM

The tests were conducted in the Langley 8-foot transonic pressure tunnel which is a single-return tunnel having a rectangular, slotted throat. In this tunnel, stagnation pressure and Mach number are independently variable; stagnation temperature is automatically held constant at 121° F. Some details of the tunnel test section have been presented in reference 7.

The models used in the present investigation were semispan models cantilevered from the tunnel sidewall. The model center line was offset 0.5 inch from the tunnel sidewall to account for the tunnel boundary layer. As shown in figure 1, a cylindrical half-body enclosed the wing root and its mounting block; ordinates for this half-body are presented in figure 2.

FLUTTER TESTS

Zero-lift flutter points were obtained at Mach numbers from 0.801 to 1.201. The procedure used in obtaining these flutter points was to increase stagnation pressure at a given Mach number until flutter was obtained. Once flutter was obtained, stagnation pressure was reduced rapidly in an effort to save the model. In each instance, however, flutter resulted in destruction of the model. Results of the flutter tests are presented in table III.

PRESENTATION OF RESULTS

The results of the present investigation are presented in figure 5 as the variation with Mach number of the correlation parameter $\frac{V_f}{b_0\omega_\alpha\sqrt{\mu_f}}$

for each wing series and are compared in figure 6(a) in terms of the flutter dynamic pressure q_f for a representative wing of each series. The q_f boundaries were computed from the boundaries of figure 5 by means of the following relationship:

$$q_f = \left(\frac{V_f}{b_0\omega_4\sqrt{\mu_f}}\right)^2 (b_0\omega_4)^2\left(\frac{m}{2v}\right)$$

Wing I9 was chosen as being representative of series I and III since the wings of these series were essentially the same and differed only by the addition of the lightweight nacelles which did not significantly alter the stiffness or mass distributions. Wing III was chosen as representative of the series II wings. Included in figure 6(b) are plots of the flutter frequency ratio ω_f/ω_4 against Mach number for the series of three wings.

DISCUSSION OF RESULTS

From the flutter boundaries of figure 6(a) it may be seen that the data for the series I (basic wing) and III (lightweight nacelles only) wing coalesce at Mach numbers from 0.80 to 0.975. This coalescence indicates no subsonic aerodynamic effect of the nacelles. At $M > 0.975$, the series III wing undergoes a significant increase in flutter dynamic pressure q_f whereas the increase in q_f for the basic wing is slight. Examination of the curves of figure 6(b) shows that the series III wing underwent a transonic change in flutter frequency ratio ω_f/ω_4 whereas the series I wing did not. These data show that the nacelles produced a favorable aerodynamic effect at Mach numbers above 0.975. Since aerodynamic theories of unsteady wing-body interference are still in an early stage of development, it is difficult to give a coherent explanation of the phenomena responsible for this nacelle effect. The present results apply, of course, only to the particular configuration tested and it seems possible that slight changes in nacelle geometry may significantly alter the effect of the nacelles on flutter. These results do indicate, however, that the supersonic flutter boundary of a highly swept wing may be significantly raised by the creation of favorable interference fields.

From figure 6(a) it is seen that the series II (engine masses and nacelles) wing exhibits only small variations of q_f with M, except for a marked increase between Mach numbers 0.96 and 1.0, where the flutter frequency also increased considerably (fig. 6(b)). The wing

with masses and nacelles (series II) had a higher flutter q_f (fig. 6(a)) than did the basic wing throughout the Mach number range investigated. At Mach numbers less than 0.975, this increase in q_f may be attributed to the addition of the engine masses since the nacelles did not affect the flutter boundary. At $M > 1.05$, q_f for the wing with masses and nacelles is greater than that for the basic wing but less than that for the wing with nacelles only. In this Mach number range no conclusions may be drawn regarding the effects of the engine masses on the basic wing; however, the addition of engine masses reduced the q_f of the wing with nacelles.

In comparing the q_f boundary of a series II model with those of series I and III models, it must be noted that the change in q_f may be due in part to a mass ratio effect which cannot be explicitly determined from the present data.

The subsonic increase in q_f resulting from the addition of the engine masses is unexpected since previous data, both experimental and theoretical, have indicated that the addition of large masses along a wing trailing edge would result in a reduced q_f. It should be noted, however, that the majority of these prior investigations dealt with wings of moderate sweep angle. Most previous theoretical analyses were based on an aerodynamic strip theory in which the spanwise component of the downwash was neglected. Moreover, the experimental data which corroborated these theoretical analyses were obtained from wings for which such an assumption is justified. In the present investigation, it is believed that the contribution of the spanwise flow to the unsteady aerodynamic forces is not negligible. It would seem, then, that the effects of localized masses on highly swept wings may be quite different from the effects of such masses on wings having smaller sweep angles. In any case, the results of the present investigation demonstrate that there exist particular configurations for which the addition of localized masses near the wing trailing edge is not detrimental.

CONCLUDING REMARKS

Three series of semispan cantilevered arrow wings which had a leading-edge sweep angle of 72.5° were flutter tested at Mach numbers from 0.801 to 1.201. The wings of the first series were basic wing panels, those of the second series carried simulated engine masses and nacelles located at 34.9, 55.8, and 76.6 percent of the semispan, and the wings of the third series carried only lightweight nacelles. The mass of each simulated engine was approximately 41 percent of the basic wing-panel mass.

At Mach numbers above 0.975, the addition of the engine masses increased the flutter dynamic pressure of the basic wing which indicated that the supersonic flutter boundary of a highly swept wing may be significantly raised by the creation of favorable interference fields. At Mach numbers above 1.03 the addition of engine masses reduced the flutter dynamic pressure of the wings carrying nacelles.

At Mach numbers below 0.975 the flutter boundaries for the basic wings and the wings with only nacelles coalesced; this indicated that there was no aerodynamic effect of the nacelles. In this Mach number range the addition of engine masses increased the flutter dynamic pressure of the basic wings, which indicated that the effect of localized masses on the flutter characteristics of highly swept wings may be quite different from the effect of such masses on wings of small sweep angle which, in general, experience a reduction in flutter dynamic pressure with the addition of trailing-edge mass.

Langley Research Center,
National Aeronautics and Space Administration,
Langley Air Force Base, Va., December 11, 1961.

REFERENCES

1. Gaukroger, D. R.: Wind-Tunnel Tests on the Effect of a Localised Mass on the Flutter of a Swept-Back Wing With Fixed Root. R. & M. No. 3141, British A.R.C., 1960.

2. Lambourne, N. C., and Weston, D.: An Experimental Investigation of the Effect of Localised Masses on the Flutter of a Model Wing. R. & M. No. 2533, British A.R.C., 1944.

3. Wilts, C. H.: Incompressible Flutter Characteristics of Representative Aircraft Wings. NACA Rep. 1390, 1958. (Supersedes NACA TN 3780.)

4. Runyan, Harry L., and Sewall, John L.: Experimental Investigation of the Effects of Concentrated Weights on Flutter Characteristics of a Straight Cantilever Wing. NACA TN 1594, 1948.

5. Staff of the NASA: Compilation of Papers Summarizing Some Recent NASA Research on Manned Military Aircraft. NASA TM X-420, 1960.

6. Woolston, Donald S., and Sewall, John L.: Use of the Kernel Function in a Three-Dimensional Flutter Analysis With Application to a Flutter-Tested Delta-Wing Model. NACA TN 4395, 1958.

7. Mugler, John P., Jr.: Transonic Wind-Tunnel Investigation of the Aerodynamic Loading Characteristics of a 60° Delta Wing in the Presence of a Body With and Without Indentation. NACA RM L55G11, 1955.

TABLE I.- MASS PROPERTIES OF MODELS

Model	Complete panel mass, slugs	Simulated engine masses, slugs			Nacelle masses, slugs			Core density, ρ_c, slugs/in.^{3}	Skin density, ρ_s, slugs/in.^{3}
		Inboard	Middle	Outboard	Inboard	Middle	Outboard		
I1	0.00810							0.948×10^{-4}	(a)
I2	.00838							1.02	0.00455
I3	.00772							.975	.00411
I4	.00812							.933	.00451
I9	.00816							.952	.00450
I10	.00836							.991	.00458
II1	.01930	0.00352	0.00352	0.00352	0.000116	0.000116	0.000116	.953	.00456
II2	.02090	.00352	.00352	.00352	.000137	.000144	.000123	.965	.00587
II3	.01940	.00352	.00352	.00352	.000123	.000123	.0000890	.928	.00478
II4	.01960	.00352	.00352	.00352	.000116	.000130	.000110	.933	.00493
II5	.01960	.00352	.00352	.00352	.000116	.000103	.0000959	.933	.00498
II6	.01960	.00352	.00352	.00352	.0000959	.000110	.0000959	.894	.00507
III1	.00912				.000116	.000116	.000116	(a)	(a)
III2	.00828				.000116	.000116	.000116	.845	.00453
III3	.00898				.000116	.000116	.000116	.929	.00491
III4	.00868				.000116	.000116	.000116	.988	.00456

[a]Data not obtained.

TABLE II.- NATURAL FREQUENCIES AND STRUCTURAL DAMPING COEFFICIENTS

Model	Natural frequencies, cps				Damping coefficients			
	f_1	f_2	f_3	f_4	g_1	g_2	g_3	g_4
I1	26.1	110	251	362	(a)	(a)	(a)	(a)
I2	25.2	108	253	364	0.0135	0.0112	0.0177	0.0183
I3	26.0	109	253	370	.0153	.0113	.0217	.0193
I4	26.0	113	250	360	.0142	.0115	.0216	.0171
I9	25.2	106	248	360	(a)	(a)	(a)	(a)
I10	25.2	108	250	360	(a)	(a)	(a)	(a)
II1	14.0	70.0	158	188	.0185	.0215	.0193	.0242
II2	14.8	71.5	160	190	.0171	.0216	.0194	.0177
II3	16.5	71.0	162	193	.0179	.0200	.0177	.0188
II4	14.5	69.7	157	190	.0169	.0184	.0183	.0195
II5	15.2	72.0	161	194	.0163	.0168	.0193	.0184
II6	14.6	71.1	158	188	.0161	.0180	.0171	.0163
III1	27.0	116	264	348	.0176	.0142	.0132	(a)
III2	26.3	111	257	348	.0168	.0142	.0130	(a)
III3	27.6	119	270	345	.0150	.0115	.0148	(a)
III4	27.6	118	265	345	.0158	.0137	.0168	(a)

[a]Data not obtained.

TABLE III.- FLUTTER TEST DATA

Model	M	ρ_f, slugs/ft^3	q_f, lb/ft^2	μ_f	f_f, cps	f_f/f_4	$V_f/b_o\omega_4\sqrt{\mu_f}$	Comments
I2	0.803	0.00254	1,009	10.4	92.3	0.256	0.172	Flutter
I3	.902	.00191	932	12.7	95.5	.258	.170	Flutter
I4	.984	.00176	990	14.5	95.0	.264	.175	Flutter
I9	1.201	.00133	1,038	19.2	97.7	.271	.179	Flutter
I10	1.102	.00157	1,070	16.7	97.0	.269	.180	Flutter
II1	.801	.00269	1,067	22.5	57.7	.307	.226	Flutter
II2	.907	.00242	1,181	27.1	57.4	.302	.226	Flutter
II3	1.103	.00183	1,248	33.2	67.5	.350	.236	Flutter
II4	1.002	.00204	1,190	30.1	60.5	.318	.234	Flutter
II6	.964	.00199	1,083	30.9	56.1	.298	.226	Flutter
III1	.850	.00237	1,043	12.1	98.0	.282	.176	Flutter
III2	.947	.00176	938	14.7	94.8	.272	.175	Flutter
III3	1.201	.00160	1,248	17.6	108	.313	.195	Flutter
III4	1.104	.00176	1,198	15.5	107	.310	.195	Flutter
II5	[a]1.198	[a].00160	[a]1,251	[a]38.3	(b)	(b)	[a].235	No flutter

[a]Conditions existing at no-flutter point.
[b]Data not obtained.

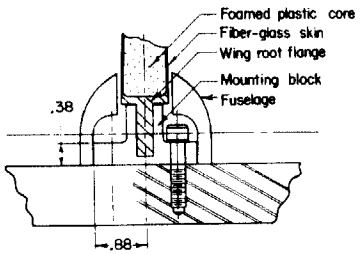

Section A-A

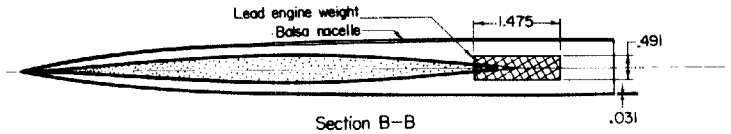

Section B-B

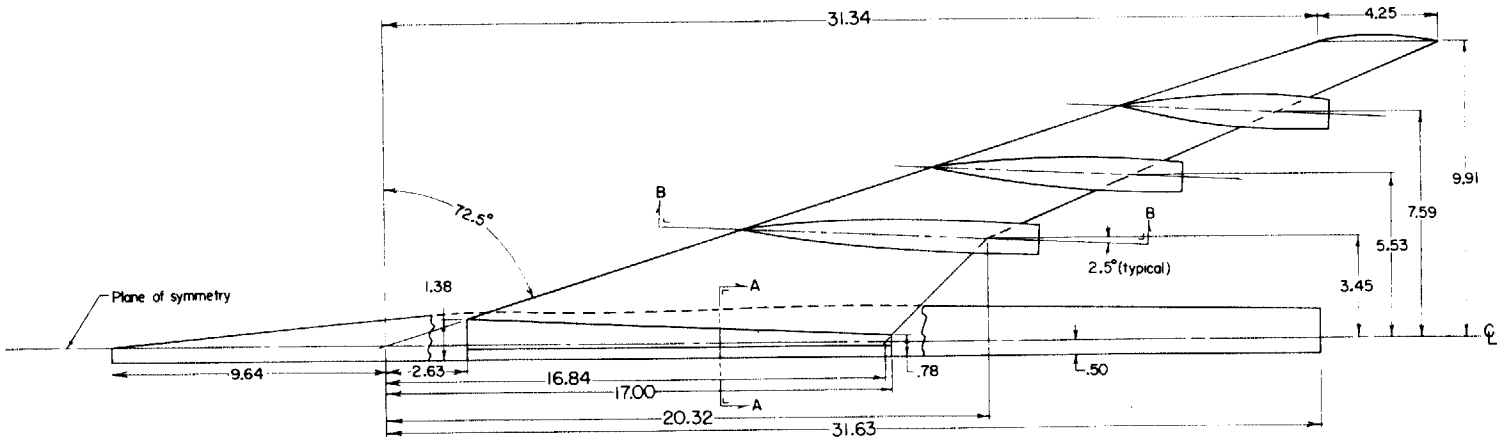

Figure 1.- Structural and geometric details of models. A = 2.29; S = 1.252 sq ft.
(All dimensions are in inches unless otherwise specified.)

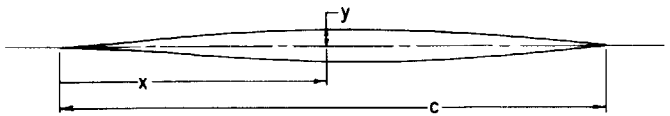

x/c, percent chord	y/c, percent chord	x/c, percent chord	y/c, percent chord
0	0.001	0.550	0.030
.050	.002	.600	.029
.100	.005	.650	.027
.150	.008	.700	.024
.200	.013	.750	.021
.250	.017	.800	.017
.300	021	.850	.013
.350	.024	.900	.009
.400	.028	.950	.005
.450	.030	1.000	0
.500	.030		

(a) Streamwise airfoil ordinates.

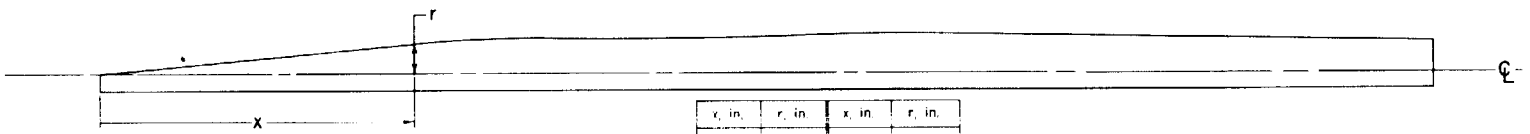

x, in.	r, in.	x, in.	r, in.
0	0	20.64	1.160
9.64	.870	21.64	1.195
10.64	.950	22.64	1.215
11.64	1.040	23.64	1.230
12.64	1.080	24.64	1.235
13.64	1.065	26.64	1.235
14.64	1.045	27.64	1.225
15.64	1.040	32.64	1.120
17.64	1.065	41.00	.930

(b) Fuselage ordinates.

Figure 2.- Airfoil, fuselage, and nacelle ordinates.

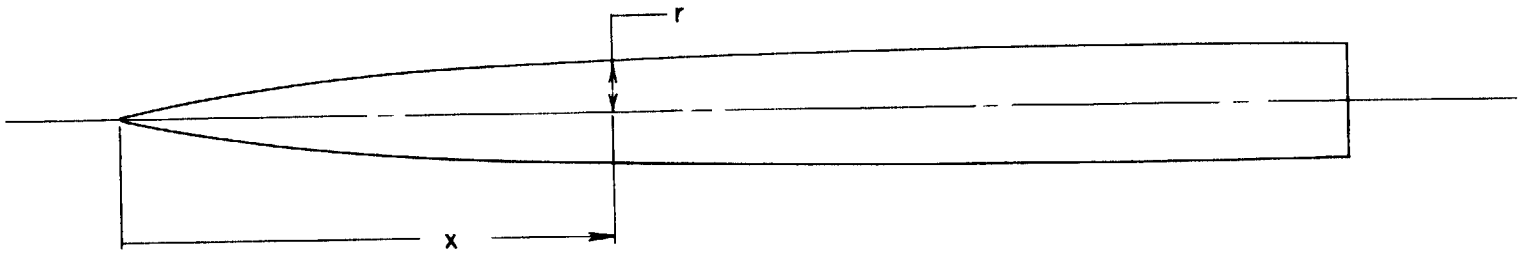

Nacelle Ordinates

Inboard nacelle		Middle nacelle		Outboard nacelle	
x, in.	r, in.	x, in.	r, in.	x, in.	r, in.
0	0	0	0	0	0
.500	.110	.500	.115	.500	.120
1.000	.195	1.000	.205	1.000	.210
1.500	.260	1.500	.275	1.790	.315
2.000	.310	2.000	.320	2.790	.400
2.725	.360	2.258	.340	3.790	.450
3.725	.400	3.258	.390	4.790	.480
4.725	.420	4.258	.430	5.440	.485
5.725	.440	5.258	.455	6.290	.480
6.725	.460	6.258	.475	7.090	.452
7.725	.470	6.908	.475		
8.375	.485	7.758	.480		
9.225	.480	8.558	.452		
10.025	.452				

(c) Nacelle ordinates.

Figure 2.- Concluded.

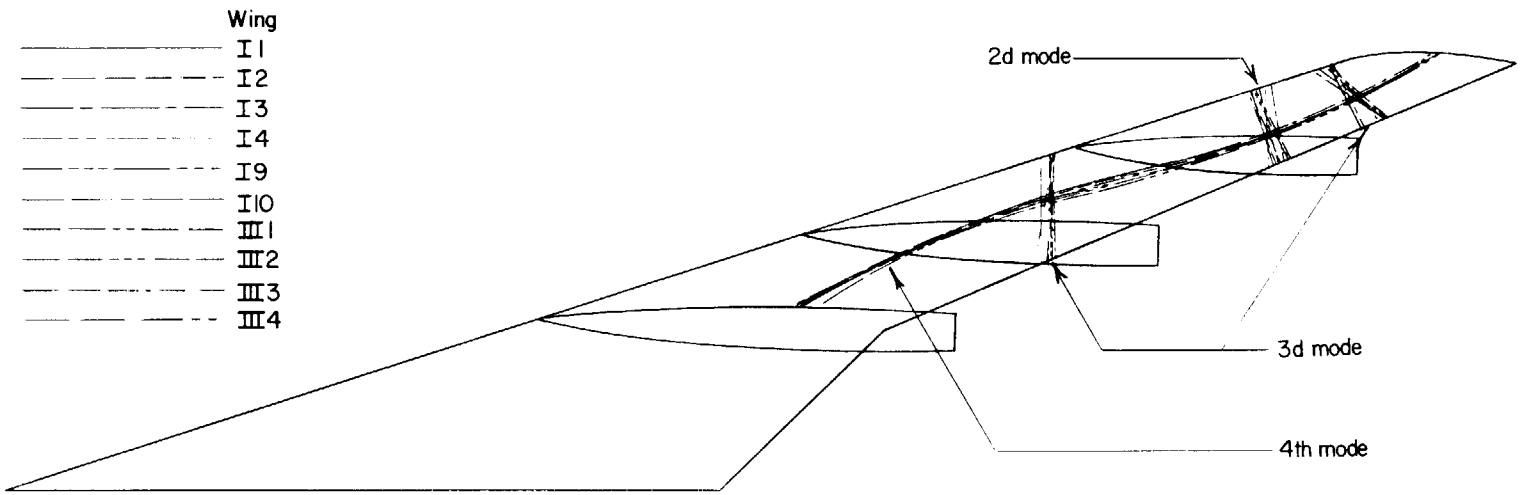

(a) Series I and III wings.

Figure 3.- Nodal patterns.

(b) Series II wings.

Figure 3.- Concluded.

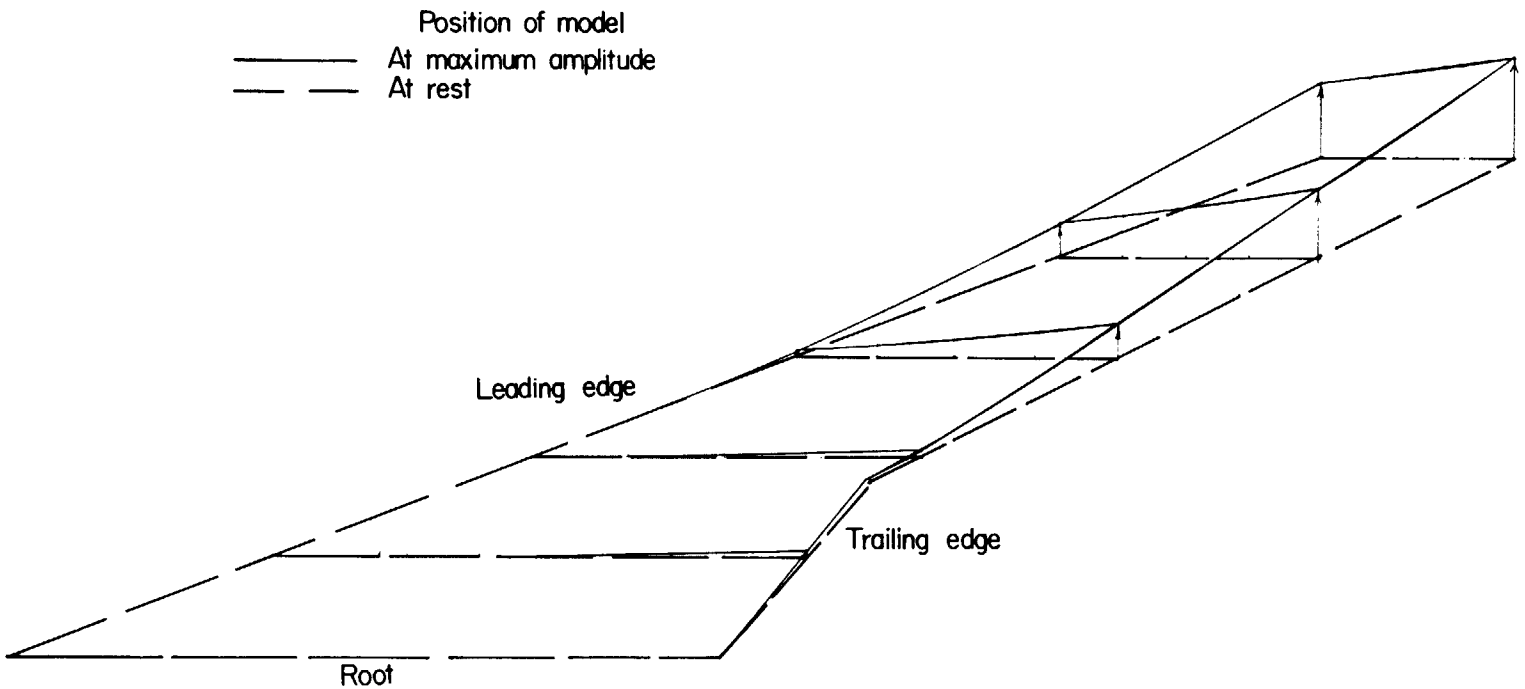

(a) First mode, series I and III wings.

Figure 4.- Experimentally determined natural mode shapes.

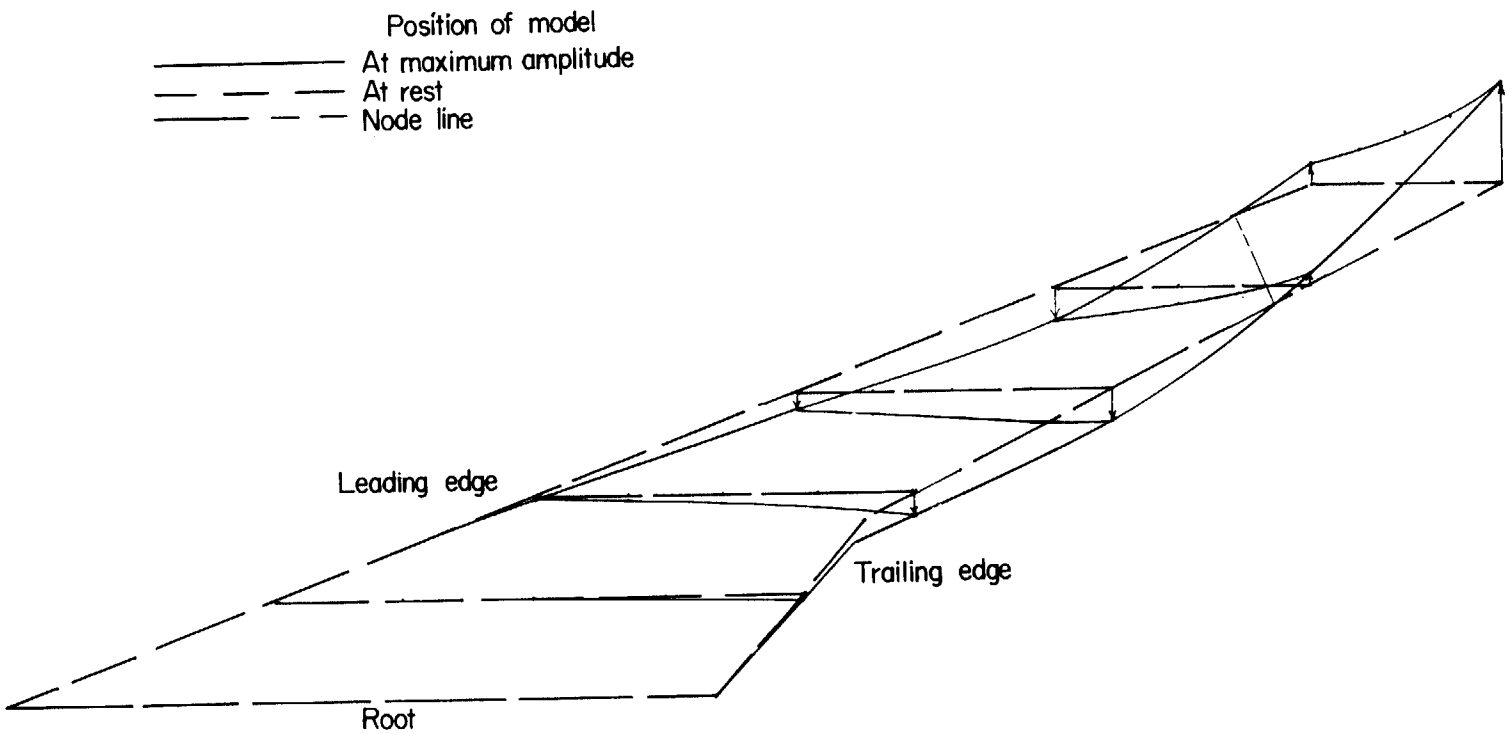

(b) Second mode, series I and III wings.

Figure 4.- Continued.

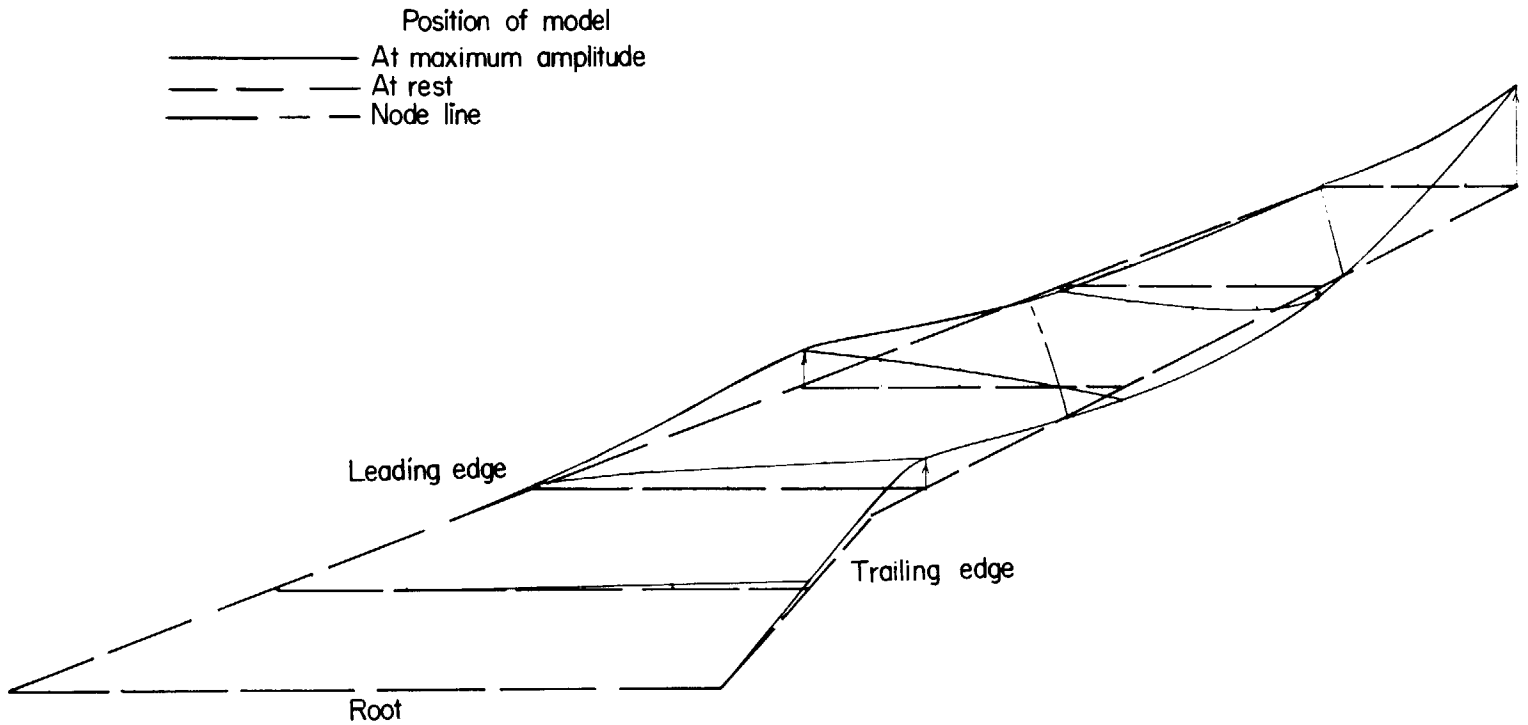

(c) Third mode, series I and III wings.

Figure 4.- Continued.

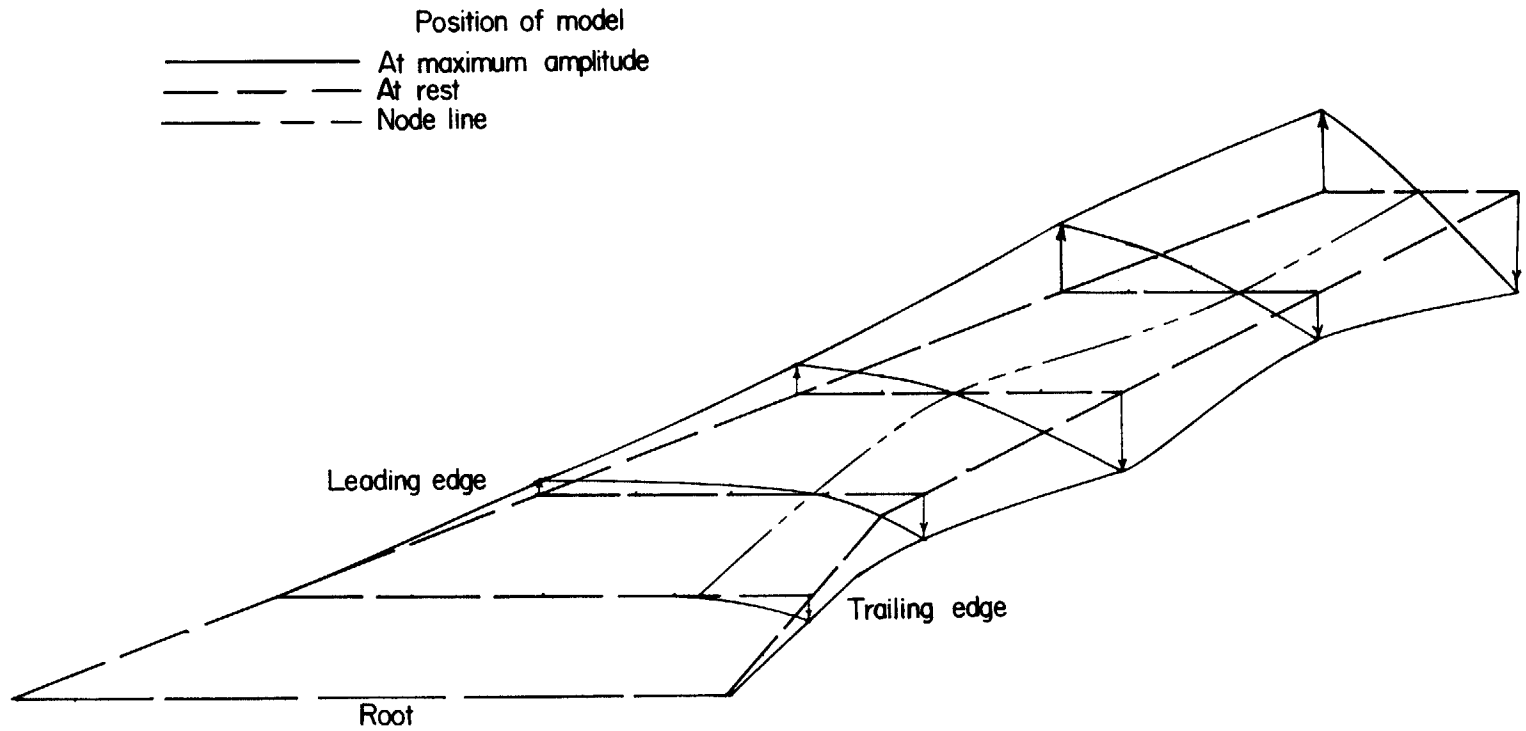

(d) Fourth mode, series I and III wings.

Figure 4.- Continued.

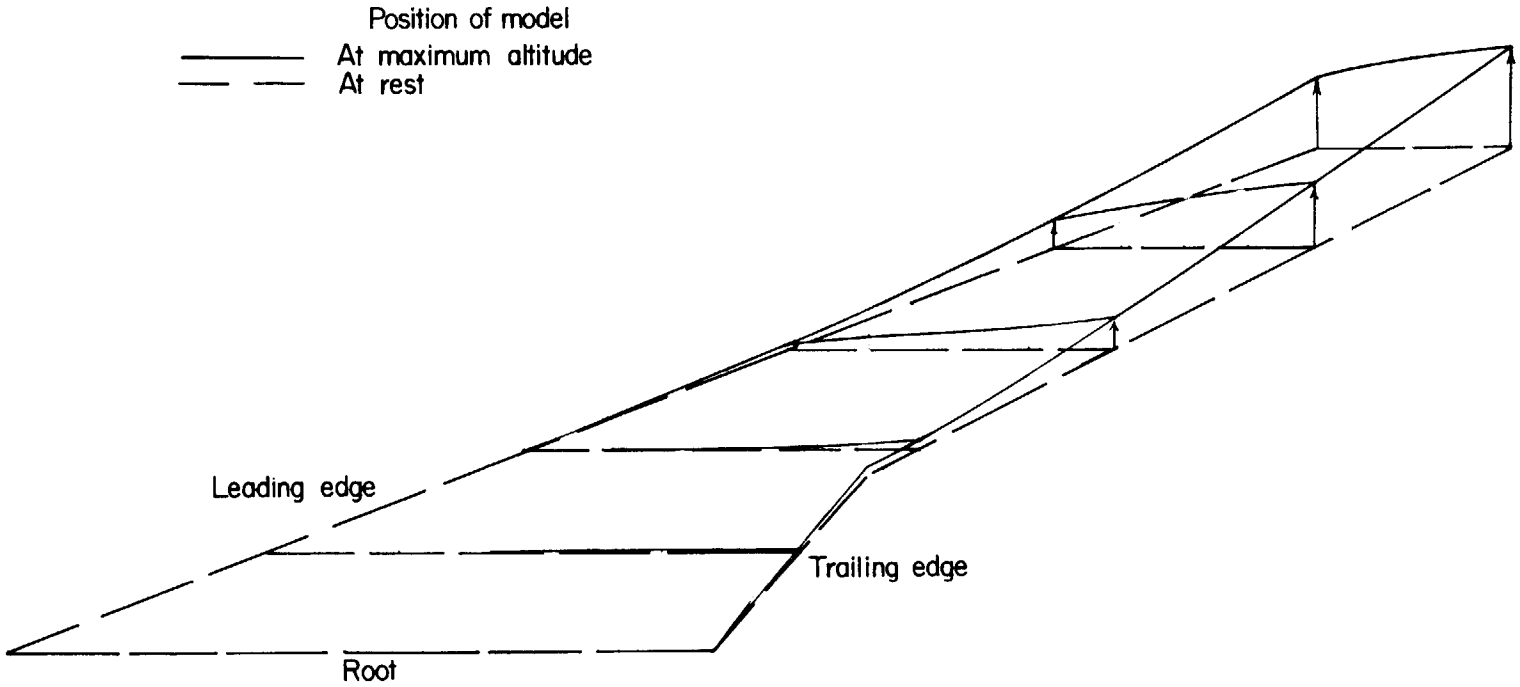

(e) First mode, series II wing.

Figure 4.- Continued.

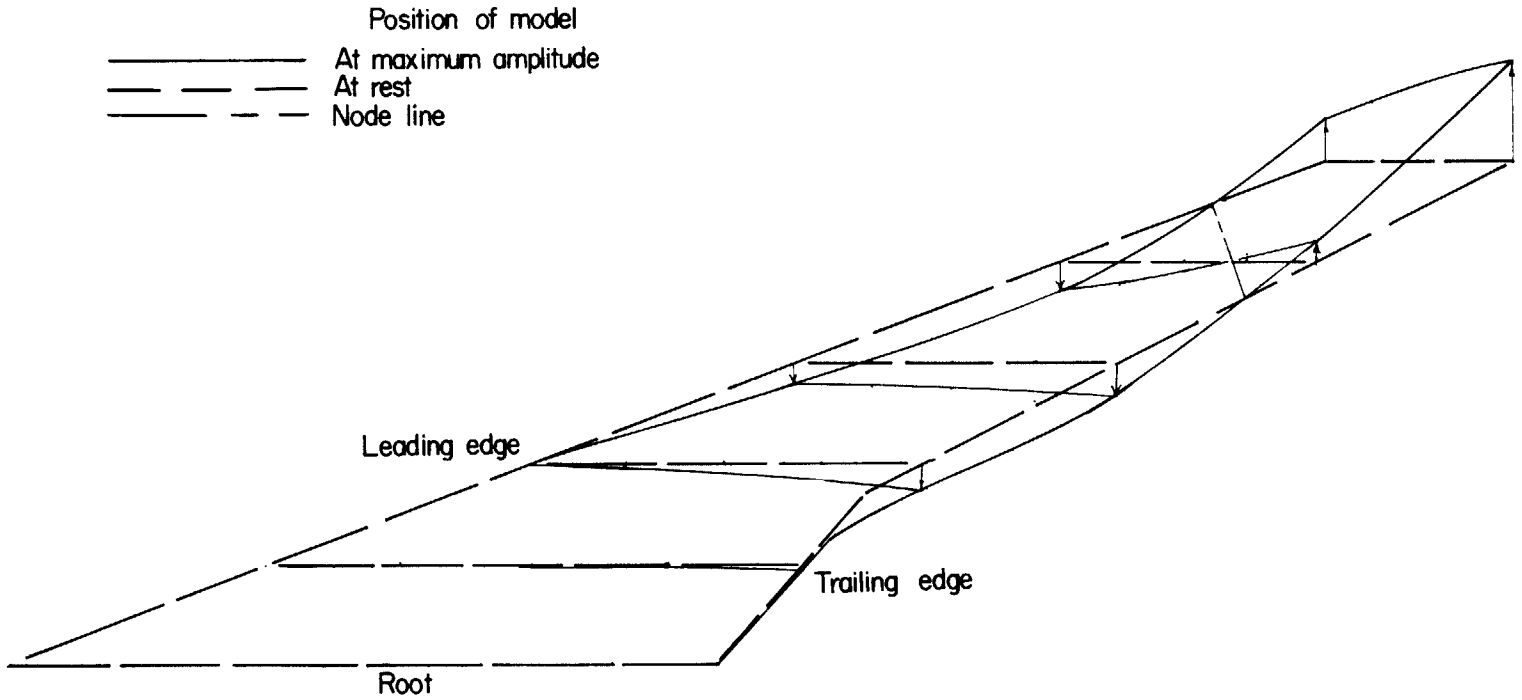

(f) Second mode, series II wing.

Figure 4.- Continued.

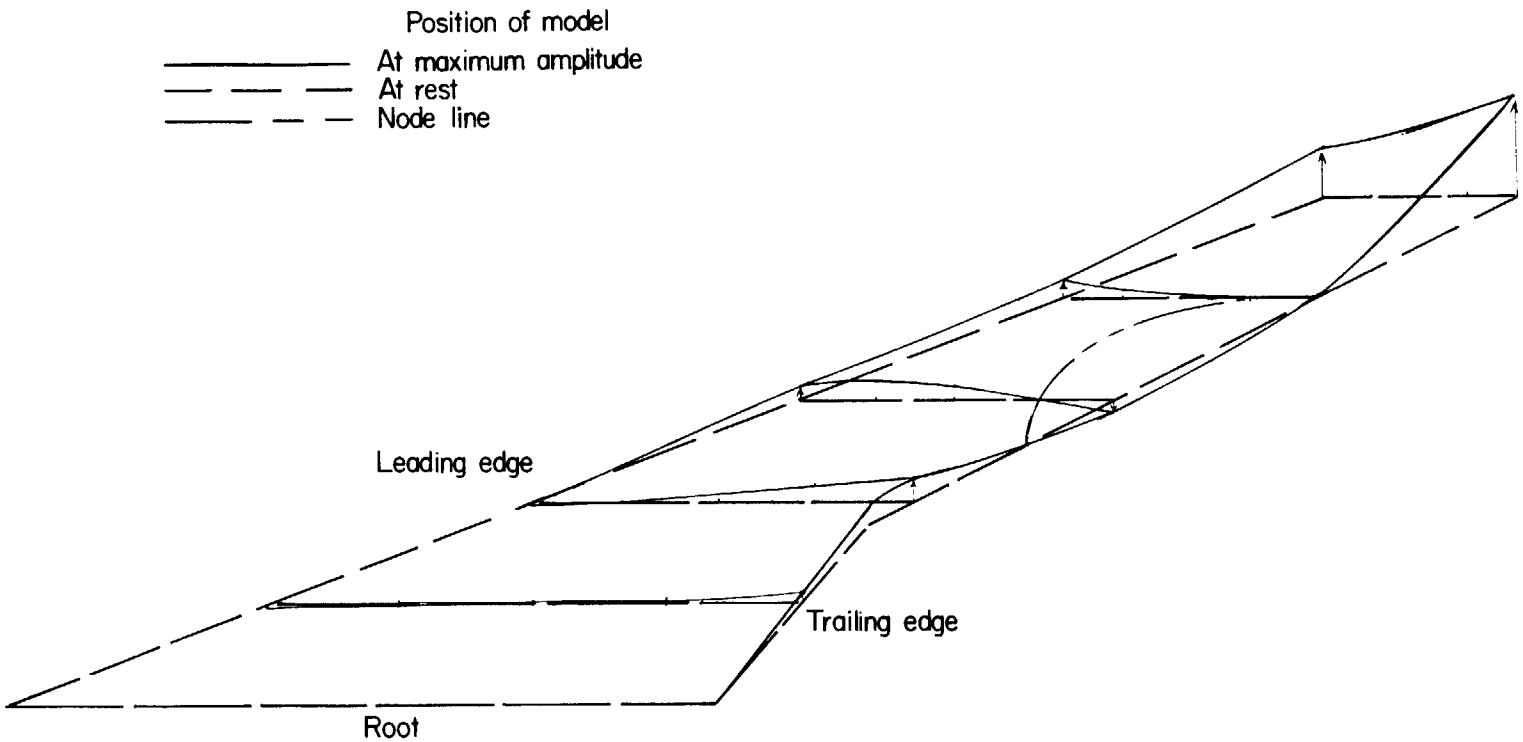

(g) Third mode, series II wing.

Figure 4.- Continued.

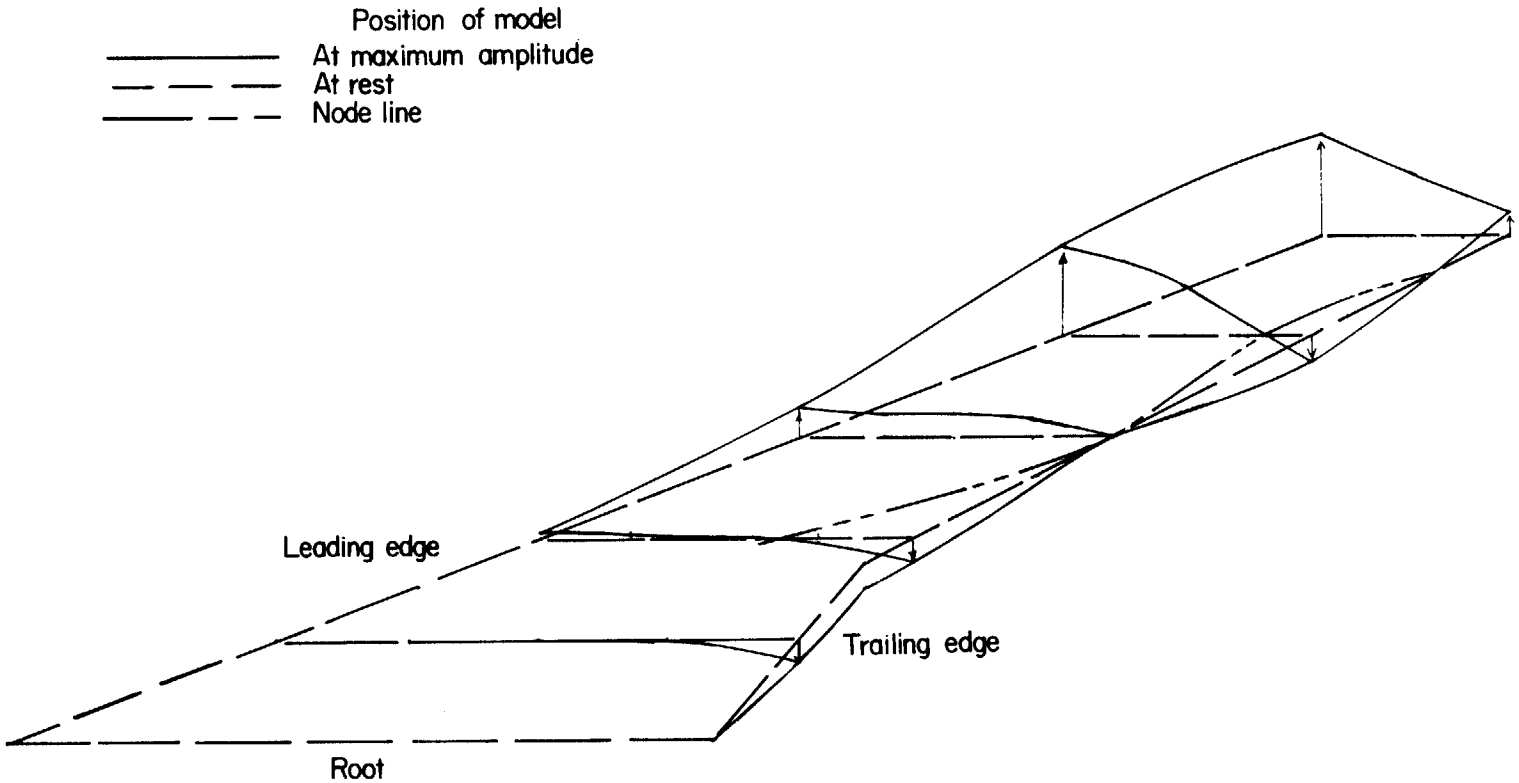

(h) Fourth mode, series II wing.

Figure 4.- Concluded.

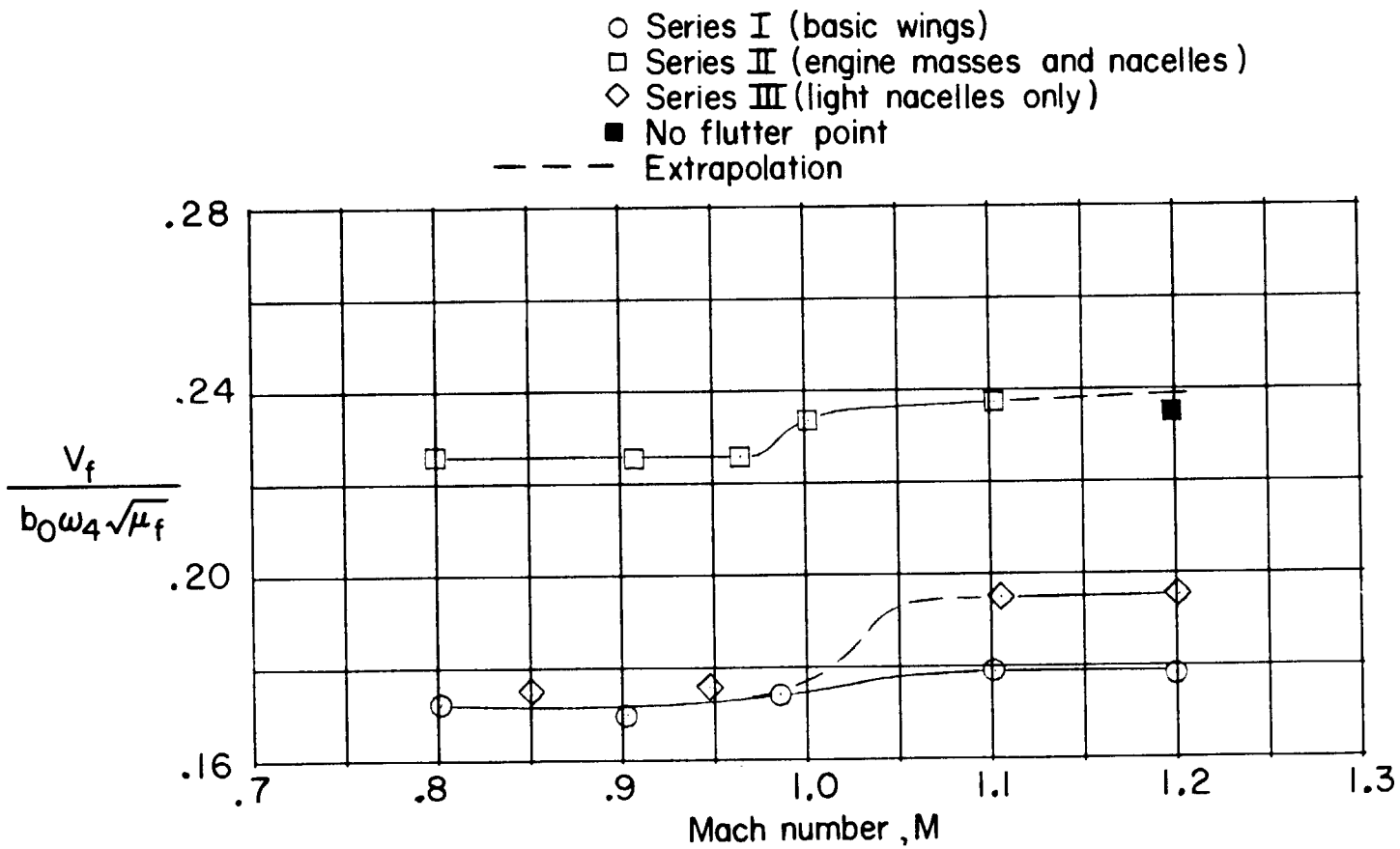

Figure 5.- Variation with Mach number of flutter speed parameter, $\frac{V_f}{b_0\omega_4\sqrt{\mu_f}}$.

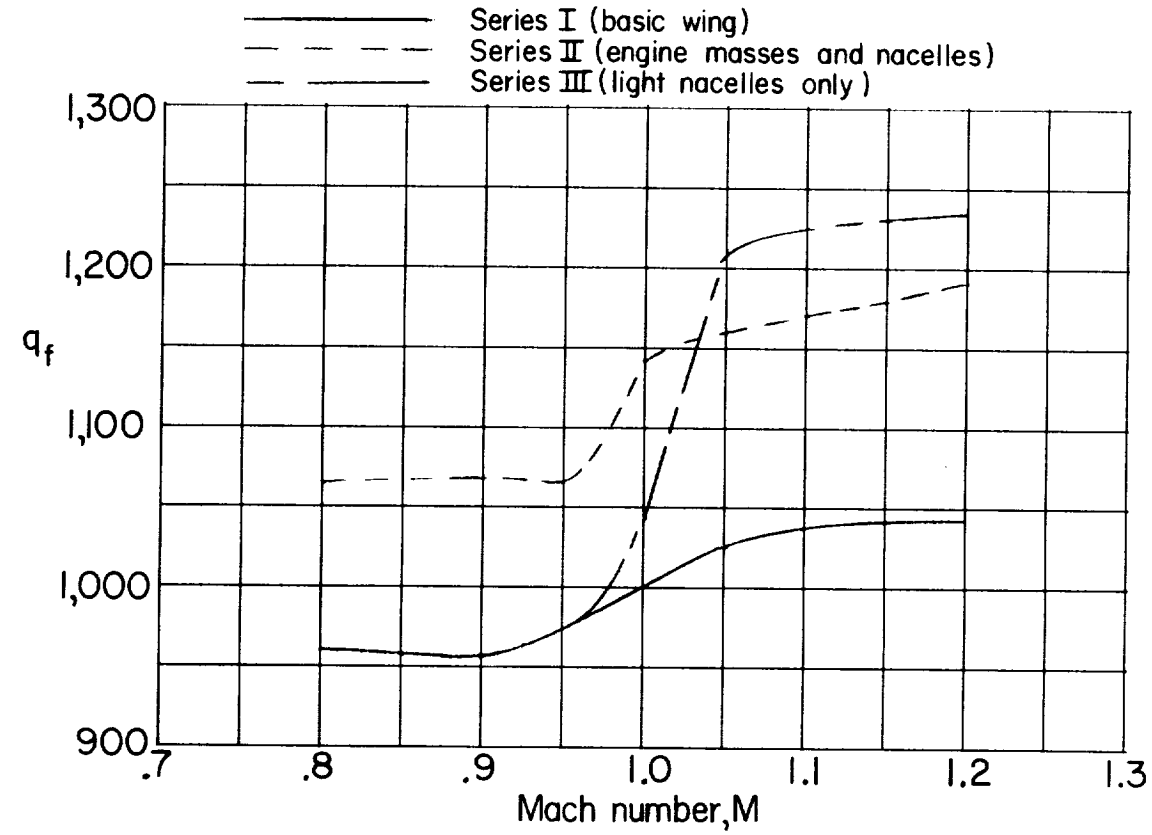

(a) Variation with Mach number of dynamic pressure required for flutter.

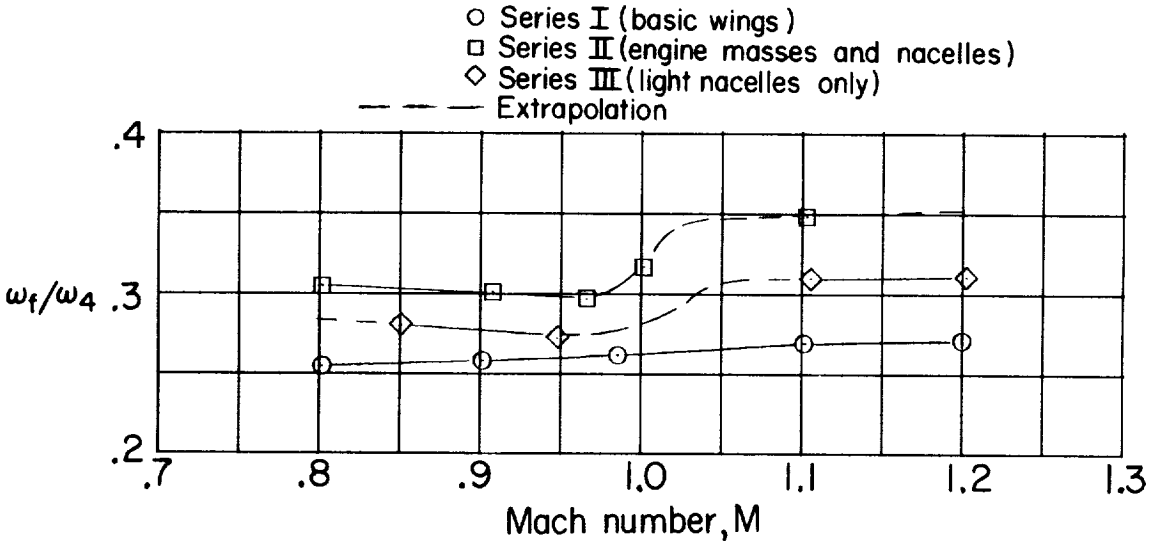

(b) Variation with Mach number of flutter-frequency ratio, ω_f/ω_4.

Figure 6.- Flutter boundaries for representative wings.

NASA-Langley, 1962 L-1654

L-1654